ELSEVIER

Materials Science and Engineering A 445–446 (2007) 186–192

MATERIALS SCIENCE & ENGINEERING A

www.elsevier.com/locate/msea

Plastic instabilities and dislocation densities during plastic deformation in Al–Mg alloys

Győző Horváth, Nguyen Q. Chinh *, Jenő Gubicza, János Lendvai

Department of Materials Physics, Eötvös Loránd University, Pázmány P. sétány 1/A., 1117 Budapest, Hungary

Received 12 July 2006; received in revised form 28 August 2006; accepted 10 September 2006

Abstract

Plastic deformation of Al–Mg alloys were investigated by analyzing the stress–strain curves obtained in uniaxial compression tests at constant loading rate. Experimental results have shown the well-known phenomenon of plastic instabilities – the Portevin–Le Chatelier effect – in these solid solution alloys. Using the characteristics of plastic instabilities – the local stress increment, $\Delta\sigma$, – dislocation densities were calculated and compared with those determined by considering the global strain hardening. The influence of the increasing Mg concentration on the multiplication and the annihilation of dislocations, as well as on the development of the mobile and immobile dislocation densities was also analyzed.

Keywords: Al–Mg alloys; Plastic instabilities; Dislocation densities

1. Introduction

Plastic instabilities as the phenomenon of discontinuous yielding – often called as Portevin–Le Chatelier (PLC) effect – manifest themselves as local stress drops ($\Delta\sigma$) or strain increments ($\Delta\varepsilon$) during uniaxial tensile stress with constant strain rate [1–5] or constant stress rate [2,5–8], respectively. Recently, the phenomenon was also investigated by depth sensing indentation (DSI) tests performed with constant loading rate, where plastic instabilities are characterized by load (ΔF) or hardness (ΔH) increments [9–15]. It is also well-known that this behavior is a consequence of the dynamic strain ageing (DSA), the effect caused by dynamic interaction between mobile dislocations and fast diffusing solute atoms. In a solid solution crystal the blocked mobile dislocations get through the obstacles in a thermally activated process for a certain waiting time (t_w). After this they traverse a certain distance (L), as a free path, until the next blocking in a negligible short flight time. In the presence of DSA the fast diffusing solute atoms give an excess blocking strength fixing the mobile dislocation better during the waiting time which can lead to negative strain rate sensitivity. Consequently, the DSA modifies the average waiting time of dislocations, hence the waiting time can be considered as a characteristic quantity describing the effectiveness of DSA.

The waiting time is a microscopic quantity which can be related to measurable macroscopic quantities of plasticity. Considering the relationship between the average velocity of dislocation motion, v, and the waiting time, $t_w = L/v$, taking into account also the Orowan equation, $\dot{\varepsilon} = \rho_m b v$, and $L = \rho_f^{-1/2}$, the waiting time can be given as:

$$t_w = \frac{\rho_m b L}{\dot{\varepsilon}} = \frac{b\rho_m \rho_f^{-1/2}}{\dot{\varepsilon}} = \frac{\Omega}{\dot{\varepsilon}} \quad (1)$$

where ρ_m and ρ_f are the mobile and forest dislocation densities, respectively, b the magnitude of the Burgers vector, $\dot{\varepsilon}$ the strain rate, and Ω is the so-called elementary strain [16,17]. According to Eq. (1) the microscopic waiting time is connected with the macroscopic strain rate through the elementary strain Ω, which plays an important role in the description of plastic instabilities. In several models [16,18–21] the strain dependence of the DSA is interpreted by the strain dependence of Ω. This is the reason why describing plastic instabilities, the elementary strain is considered as a typical constitutive quantity [18,20], which has been determined experimentally with different, more or less complex methods [18–20,22].

The phenomenon of plastic instabilities is strongly related to the evolution of mobile and forest dislocation densities. Although the PLC effect in Al–Mg has been extensively

* Corresponding author. Tel.: +36 1 372 2845; fax: +36 1 372 2811.
E-mail address: chinh@metal.elte.hu (N.Q. Chinh).

0921-5093/$ – see front matter © 2006 Elsevier B.V. All rights reserved.
doi:10.1016/j.msea.2006.09.019

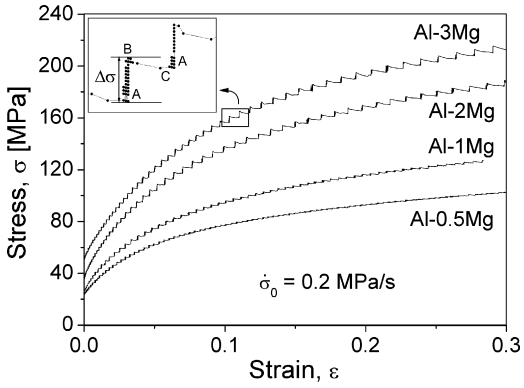

Fig. 1. Stress–strain curves for different Mg concentrations. The inset shows a stress increment, $\Delta\sigma$ associated with the DSA effect.

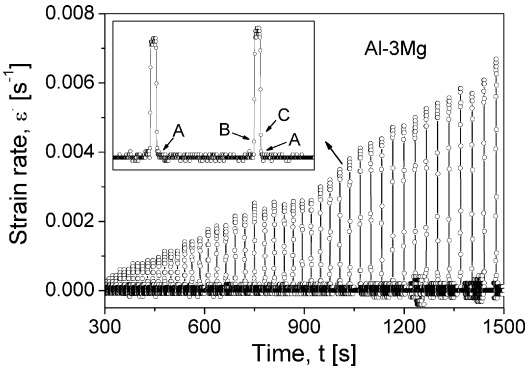

Fig. 2. Strain rate as a function of time for Al–3Mg. The inset shows the strain rate peak according to the inset in Fig. 1.

investigated, no systematic study of the development of mobile and forest dislocations as a function of Mg concentration has been published.

In this paper the characteristics of plastic instabilities occurring in Al–Mg solid solution alloys deformed by stress-controlled uniaxial compression tests are investigated. By analyzing these characteristics, the development of mobile and immobile dislocation densities are estimated and compared with those obtained by other methods. The effect of Mg addition on the development of both dislocation densities is also discussed.

2. Experimental

Compression measurements were carried out on binary Al–Mg alloys with 0.5, 1, 2 and 3 wt.% Mg. All samples were solution heat treated at 470 °C for 30 min and water-quenched to room temperature. Cylindrical samples with diameter of 6 mm and height of 8 mm were worked out for uniaxial compression tests, which were performed on an MTS 810 servohydraulic testing machine at room temperature with constant loading rates of 0.5, 5 and 50 N/s, which correspond to the initial stress rates, $\dot{\sigma}_0$ of 0.02, 0.2 and 2 MPa/s, respectively. During measurements the imposed load and displacement of the compressing head were recorded as a function of time, with the sampling frequency up to 100 Hz. It should be noted that the real stress-controlled tests are very sensitive on the control parameters of the testing machine drive [5,23], mainly in the case of tensile test. Although, it can be improved by using implemented soft elements in series to the specimen [5], the solution still remains very complicated, even when using relatively fast control system. In the present investigation, therefore, we applied the electronically well-controllable load-controlled system for compression tests.

3. Experimental results

Fig. 1 shows some typical stress–strain curves obtained at $\dot{\sigma}_0 = 0.2$ MPa/s for different Mg-containing Al–Mg alloys. On the one hand, the global shape of these curves show the well-established strengthening effect of Mg addition [14] manifested by the increase of both the proof stress and flow stress with increasing Mg concentration. On the other hand, the stress–strain curves show also plastic instabilities as local features during stress rate-controlled compression test. This phenomenon manifests itself as characteristic stress–strain steps indicating two alternating states (see inset of Fig. 1). On the steep (denoted as AB) part of the steps the strain hardly changes while the stress is monotonously increasing with a stress increment, $\Delta\sigma$. Reaching a certain stress value local softening appears inducing rapid strain change at nearly constant load, F, at regime BC. As the cross-section, A of the sample is monotonously increasing in compression measurements, the stress level ($\sigma = F/A$) is slightly decreasing at the rapid plastic event. It should be emphasized that this stress-decrease is then neither the overshoot nor the delay of the stress controlling system, which are often observed in the real stress-controlled tests [2]. Considering the process of plastic deformation in the present investigation, the strain rate, $\dot{\varepsilon}$, as a function of time, t, was calculated and plotted in Fig. 2. In this figure the plastic instabilities can also be characterized by the occurrence of the successive low (AB) and high (BC) strain rate regimes. Here we note that the step-like behavior observed during stress rate-controlled compression test is quite similar to that occurring in the indentation tests with constant loading rates [10,11].

Fig. 3 shows the σ–ε curves of Al–2Mg alloy deformed at different initial stress rates. The experimental results show that at room temperature, where the effect of thermal activation is not so strong, the stress rate has practically no influence on the global

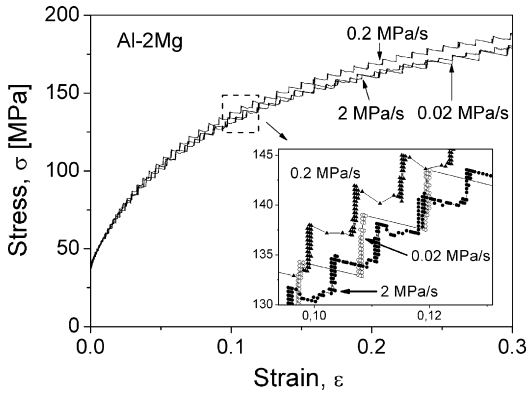

Fig. 3. The effect of stress rate on the stress–strain curves.

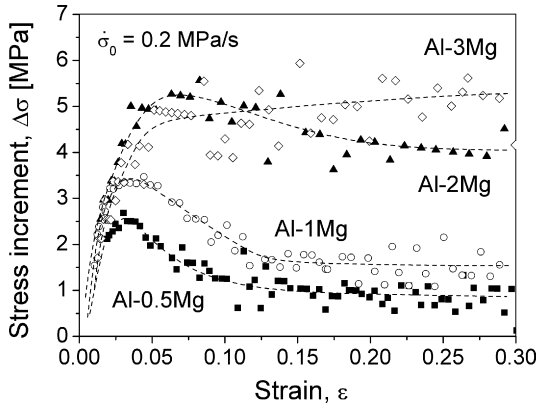

Fig. 4. The $\Delta\sigma$–ε curves obtained at $\dot{\sigma}_0 = 0.2$ MPa/s for different magnesium concentrations.

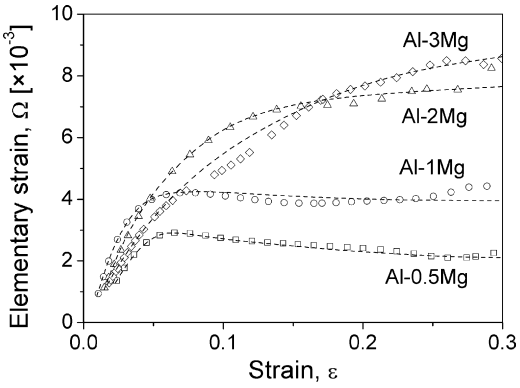

Fig. 5. The development of elementary strain, Ω during plastic deformation for different magnesium concentrations.

stress–strain relationship. At a given strain, both the flow stress and the rate of strain hardening of the global σ–ε curves remain – within statistical error – unchanged when the initial stress rate is changing from 0.02 to 2 MPa/s. In contrast to this, the local stress increment, $\Delta\sigma$ characterizing the PLC effect seems to be considerably sensitive to the stress rate, $\dot{\sigma}$. At a given strain, the lower the stress rate the larger value of $\Delta\sigma$ can be observed.

In order to characterize plastic instabilities responsible for the local plastic behavior of the samples, the height of the steps, which can be considered as the depth of DSA, appearing on the stress–strain curves were analyzed. Fig. 4 shows the development of the stress increments, $\Delta\sigma$ as a function of strain for Al–Mg alloys with different magnesium concentration deformed at an initial stress rate of $\dot{\sigma}_0 = 0.2$ MPa/s (see also Fig. 1). It can be seen that the evolution of $\Delta\sigma$ depends strongly on the Mg concentration. In the case of small Mg concentrations $\Delta\sigma$ increases at small strains and after a maximum it decreases and at high strains it becomes constant. For the highest Mg concentration the decreasing part of the curves disappears, and after the initial increasing regime saturation is found.

4. Discussion

The characteristics of $\Delta\sigma$ and the dependence of this quantity on numerous other parameters like temperature, strain rate, etc., has been investigated in several works [3,8,14,24,25]. The strain dependence of $\Delta\sigma$ has also been observed and discussed both for constant strain rate [2,4,25–27] and constant stress rate [6,7]. In these works the evolution of the instability step, $\Delta\sigma$ during plastic deformation was explained, on the one hand, by the increasing dislocation density, exhausting solute content or work hardening [2,4,21,28,29], and on the other hand, by the changing ratio of the mobile and immobile (forest) dislocation densities [16,27]. In the following, the densities of these two types of dislocations are estimated from the characteristic features of plastic instabilities for the Al–Mg alloys investigated here and the effect of Mg content on the development of these dislocation densities is discussed.

4.1. Dislocation densities calculated by using the characteristics of plastic instabilities

Considering the process of plastic deformation, the occurrence of the instability steps on the stress–strain curves is explained by the jerky motion of dislocations. The flat part of the step corresponds to the high velocity motion of dislocations, while the steep part reflects the state when the mobile dislocations are temporarily blocked by obstacles. In the latter state two basic processes contest: (i) the blocking stress is increasing with the number of solutes diffusing towards dislocations and (ii) the monotonously increasing external stress is trying to move dislocations over the obstacles. The waiting time, t_w, which characterizes the blocking process at a given step, can be estimated from the measured stress increment, $\Delta\sigma$ by the formula:

$$\Delta\sigma = \dot{\sigma} \times t_w$$

from which

$$t_w = \frac{\Delta\sigma}{\dot{\sigma}} \tag{2}$$

Determining experimentally also the global strain rate, $\dot{\varepsilon}_{glob}$ from the strain–time curve, the elementary strain, $\Omega(\varepsilon)$ as a function of the global strain can be derived from the $\Delta\sigma$–ε curves with the help of Eqs. (1) and (2):

$$\Omega(\varepsilon) = \frac{\Delta\sigma(\varepsilon) \times \dot{\varepsilon}_{glob}(\varepsilon)}{\dot{\sigma}} \tag{3}$$

Fig. 5 shows the development of the elementary strain during plastic deformation for the different Al–Mg alloys deformed at $\dot{\sigma}_0 = 0.2$ MPa/s. Experimental results show that the Ω–ε function depends strongly on the Mg concentration. At small concentrations the Ω–ε curves have a maximum which is followed by a slightly decreasing part, while for higher Mg concentrations the curves increase monotonously. It is worth mentioning at this point, that for higher magnesium content the results are in good agreement with the experimentally determined Ω–ε curves in the literature [18,19,22], while the curves for samples with lower Mg content have the same tendency as it was proposed by theoretical models [16,20].

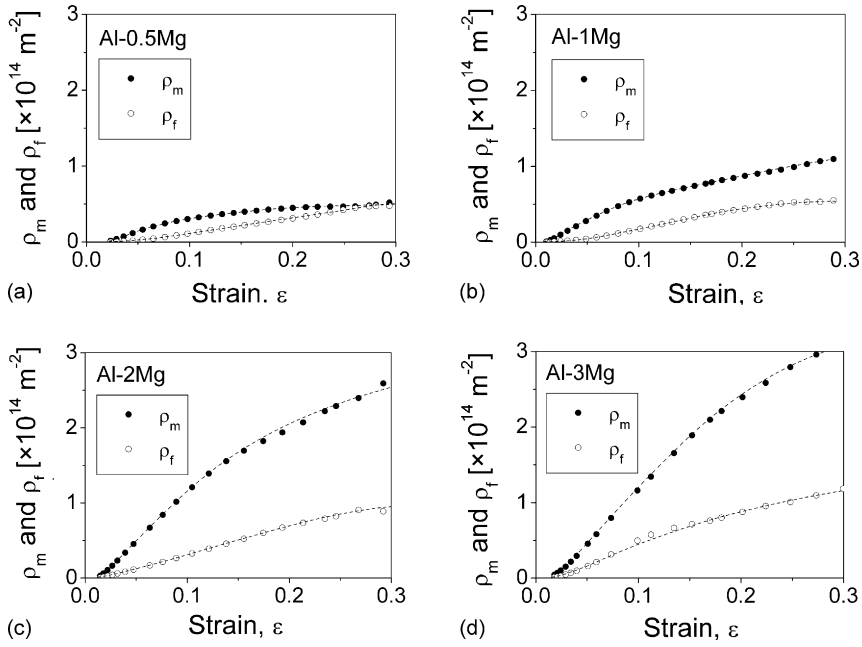

Fig. 6. The development of mobile (ρ_m) and forest (ρ_f) dislocation densities during plastic deformation at $\dot{\sigma}_0 = 0.2$ MPa/s in (a) Al–0.5Mg, (b) Al–1Mg, (c) Al–2Mg and (d) Al–3Mg alloys.

Considering the expression of the elementary strain, $\Omega = b\rho_m\rho_f^{-1/2}$ in Eq. (1) and taking into account the Taylor equation for the flow stress:

$$\sigma = \sigma_0 + \alpha MGb\sqrt{\rho} = \sigma_0 + \alpha MGb\sqrt{\rho_m + \rho_f}, \quad (4)$$

where σ_0 is the proof stress, α a constant ($\alpha = 0.33$ was taken), M the Taylor factor ($M = 3$ for untextured polycrystalline materials), G the shear modulus ($G = 26$ GPa for Al and its alloys) and $\rho = \rho_m + \rho_f$ is the total average dislocation density, the development of mobile (ρ_m) and forest (ρ_f) densities can be determined as a function of strain (Fig. 6). Both calculated dislocation densities increase with increasing Mg concentration. Furthermore, the increase of the density of mobile dislocations with increasing Mg concentration is higher than that for forest dislocations. It should be mentioned here that the total dislocation densities of 1.2×10^{14} m^{-2} and 3.1×10^{14} m^{-2} determined from the plastic instabilities in Al–1Mg and Al–3Mg at strain of 0.2 are in good agreement with the values of 0.9×10^{14} m^{-2} and 3.6×10^{14} m^{-2} determined by X-ray diffraction line profile analysis [30].

4.2. Determination of dislocation densities by taking into account major mechanisms of plastic deformation

According to the Taylor formula expressed in Eq. (4), the stress–strain connection (σ–ε curve) can be obtained theoretically by establishing the functional relationship between ρ and ε during plastic deformation. Several models have been proposed to describe the development of the dislocation density during plastic deformation [16,21,31–33] but, considering the development of both types of dislocation densities, ρ_m and ρ_f, it is reasonable to adopt the Kubin–Estrin (KE) model [16] for a more detailed analysis. In this model the development of mobile and forest dislocation densities are described by the following relationships:

$$\frac{d\rho_m}{d\varepsilon} = C_1 - C_2\rho_m - C_3\rho_f^{1/2} \quad (5a)$$

and

$$\frac{d\rho_f}{d\varepsilon} = C_2\rho_m + C_3\rho_f^{1/2} - C_4\rho_f, \quad (5b)$$

where the terms containing the parameters C_i are related to the primary microscopic processes occurring during plastic deformation such as the multiplication of mobile dislocations (C_1), their mutual annihilation and trapping (C_2), their immobilization through interactions with forest dislocations (C_3) and to the advent of dynamic recovery (C_4). The parameter C_2 is reintroduced in the equation for the evolution of the forest density to account for the creation of immobile partial dislocations and/or immobile dipolar arrangements, as well as for the formation of debris, loops left by the mutual annihilation of mobile dislocations. In the present description these quantities are considered as material constants with the note that some of them, especially C_2 and C_4 – which in fact characterize the annihilation of ρ_m and ρ_f, respectively – may depend on strain rate and temperature since they account for thermally activated mechanisms like cross-slip or climb. It was shown previously [34] that the macroscopic stress–strain relationships of pure Al and Cu can be satisfactorily described on the basis of this model.

In the present work, the values of C_i parameters were chosen so that the numerical solution of the equation system (5a) and (5b) describes best the experimental σ_p–ε relationship, where $\sigma_p = \sigma - \sigma_0 = \alpha MGb\sqrt{\rho}$ is the stress component developed during plastic deformation. The C_i values determined by this procedure are listed in Table 1. Fig. 7 shows the theoretical σ_p–ε curves obtained by using the fitted C_i values for all the

Table 1
The parameters of Eqs. (5a) and (5b) obtained from fitting to the experimental curves of Al–Mg alloys

	C_1 (m^{-2})	C_2	C_3 (m^{-1})	C_4
Al–0.5Mg	5.2×10^{14}	7.0	2.1×10^{7}	8.1
Al–1Mg	8.4×10^{14}	5.5	2.6×10^{7}	9.4
Al–2Mg	1.6×10^{15}	4.0	1.8×10^{7}	8.0
Al–3Mg	1.9×10^{15}	3.0	4.8×10^{7}	7.8

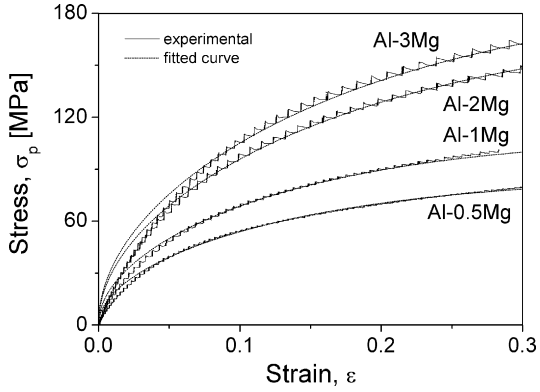

Fig. 7. The σ_p–ε curves numerically calculated by Eqs. (5a) and (5b) with experimental ones for different Mg concentrations.

Al–Mg alloys and also the corresponding experimental curves. Fig. 7 demonstrates excellent agreement with the experimental data in the case of alloys having lower Mg addition, providing support for the principles of the KE theoretical model. For higher (2% and 3%) Mg contents, however, the deviation between the experimental and the fitted line is larger. For all investigated alloys the agreement between the experimental curves and the predicted lines of the KE model seems to fail at small strains up to $\varepsilon = 0.05$, as it was observed earlier for pure Al and Cu [34].

Fig. 8 shows the development of mobile (ρ_m) and forest (ρ_f) dislocation densities as a function of strain calculated by KE model, together with that estimated by using characteristics of plastic instabilities (shown in Fig. 5). It can be seen that in the case of dilute (0.5 and 1% Mg) alloys the corresponding quantities obtained by two different ways are in excellent agreement, confirming the validity of the procedure based on the characteristics of plastic instabilities. For higher Mg contents, especially for Al–3%Mg, more significant deviations can be observed between the mentioned quantities, which may be explained by the enhanced interaction between dislocations and solute atoms. It is well-known [30] that the addition of Mg retards the recovery in Al. In the present case the dislocation–solute interaction at high Mg content may change considerably with increasing dislocation density, modifying the effect of annihilation and dynamic recovery, i.e. changing the value of C_2 and C_4 parameters as a function of strain. This may lead to the incorrect estimation of the dislocation densities by applying Eqs. (5a) and (5b) for alloys having high solute content. It should be emphasized, however, that in the case of all alloys investigated here the quantities of both ρ_m and ρ_f obtained by different ways show similar tendency in their development during plastic deformation.

4.3. The effect of Mg addition on the development of dislocation densities during plastic deformation

Considering the results obtained by using the characteristics of plastic instabilities (shown in Fig. 6), it has been mentioned that both the mobile and forest dislocation densities increase with increasing Mg concentration. Furthermore, the increment of the mobile dislocation density is higher than that of the forest dislocation density. Fig. 9 shows $P_m = \rho_m/\rho$, the ratio of the mobile to the total dislocation density. P_m decreases monotonously from 0.9 to 0.5 and to 0.65 for the Al–0.5

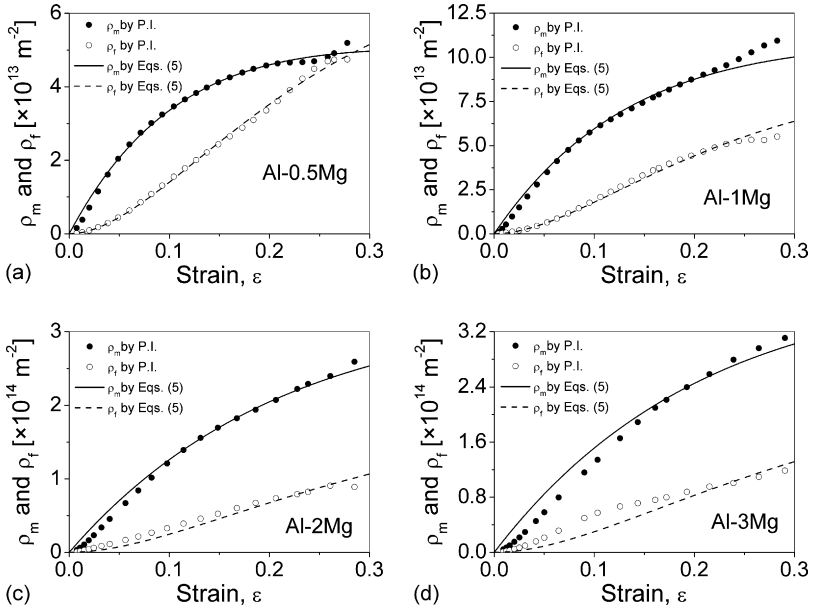

Fig. 8. The mobile (ρ_m) and forest (ρ_f) dislocation densities calculated from plastic instabilities (P.I.) and those determined by Eqs. (5a) and (5b) for (a) Al–0.5Mg, (b) Al–1Mg, (c) Al–2Mg and (d) Al–3Mg alloys.

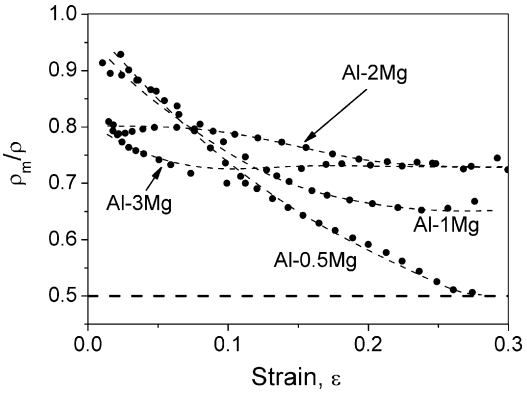

Fig. 9. The development of the ρ_m/ρ ratio during plastic deformation in Al–Mg alloys.

and Al–1Mg alloys, respectively, and it changes only slightly between 0.7 and 0.8 for the higher Mg contents of 2 and 3%.

According to the results of numerical calculations (see Table 1), it can be concluded that the Mg content enhances strongly the multiplication of the mobile dislocation density, characterized by the parameter C_1. Plotting the value of C_1 against Mg concentration, C_{Mg}, as shown in Fig. 10, an approximately linear relationship can be observed. The value of C_1 obtained by the extrapolation to zero Mg addition ($2.5 \times 10^{14}\ m^{-2}$) is close to the value obtained for pure Al [34]. Furthermore, considering the decreasing value of parameter C_2 with increasing Mg content (see Table 1), it can also be concluded that the annihilation of mobile dislocation density decreases with increasing Mg addition. On the one hand, at a given mobile dislocation density, ρ_m, the higher the Mg concentration the smaller fraction of mobile dislocations transforms into forest dislocations, and on the other hand the addition of Mg decreases the recovery of Al–Mg alloys. These phenomena together determine mainly the development of both dislocation densities. It is well-known that the Mg atoms prefer to stay at the dilated region of edge dislocations, which decreases the tensile strains around these dislocations and also hinders the non-conservative motion of dislocations [35]. As a result of the strong dislocation–solute atoms interaction, dislocations are less clustered to minimize their strain energy for higher Mg content. This

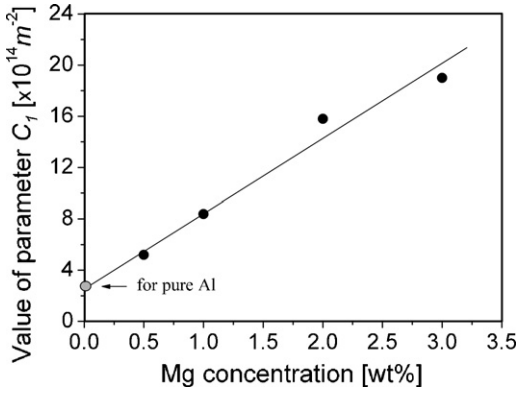

Fig. 10. The value of parameter C_1 in Eq. (5a) as function of the Mg content in Al–Mg alloys.

is supported by previous TEM studies [30,36], which revealed that the dislocation substructure in plastically deformed Al–Mg alloys with 3–6% Mg concentrations consist of a fairly uniform distribution of dislocation tangles, i.e. no expressed dislocation cell structure can be formed, while for pure Al the dislocations are arranged into cell walls even at about 5% strain. As the trapped dislocations in the cell walls are immobile [37], the relative fraction of forest dislocations is higher for lower Mg content. Another consequence of the formation of diffuse dislocation tangles is the smaller mean free path for dislocation motion in alloys having higher Mg concentration so that the dislocations intersect each other more frequently. This results in higher rate of dislocation formation by Frank-Read mechanism, leading to the higher density of mobile dislocations.

5. Conclusions

Plastic instabilities and dislocation densities in solid solution Al–Mg alloys were investigated by analyzing the stress–strain curves obtained in uniaxial compression tests at constant loading rate. The main results can be summarized as follows:

(i) The characteristics of Portevin–Le Chatelier plastic instabilities depend strongly on the Mg concentration.
(ii) Using the local stress increment of plastic instabilities, the mobile and immobile dislocation densities were calculated and compared with those determined from the global stress–strain curve. The dislocation densities obtained from the essentially different methods were in good agreement.
(iii) Increasing the Mg content in solid solution Al–Mg alloys enhances strongly the multiplication of mobile dislocations and decreases the trapping of mobile dislocations and the annihilation of immobile dislocations. This leads to the strong strengthening effect of Mg addition in Al–Mg alloys.

Acknowledgements

This work was supported by the Hungarian National Scientific Research Fund (OTKA) under contract numbers T-038048, F047057 and T-043247. J.G. is grateful for the support of the Bolyai Janos Research Scholarship of the Hungarian Academy of Sciences.

References

[1] Ch. Schwink, A. Nortmann, Mater. Sci. Eng. A234–A236 (1997) 1–7.
[2] F.B. Klose, A. Ziegenbein, J. Weidenmüller, H. Neuhäuser, P. Hähner, Computat. Mater. Sci. 26 (2003) 80–86.
[3] F.B. Klose, A. Ziegenbein, F. Hagemann, H. Neuhäuser, P. Hähner, M. Abbadi, A. Zeghloul, Mater. Sci. Eng. A369 (2004) 76–81.
[4] F.B. Klose, J. Weidenmüller, A. Ziegenbein, P. Hähner, H. Neuhäuser, Philos. Mag. 84 (3–5) (2004) 467–480.
[5] H. Neuhäuser, F.B. Klose, F. Hagemann, J. Weidenmüller, H. Dierke, P. Hähner, J. Alloy Compd. 378 (2004) 13–18.
[6] Zs. Kovács, J. Lendvai, G. Vörös, Mater. Sci. Eng. A279 (2000) 179–184.
[7] Zs. Kovács, N.Q. Chinh, J. Lendvai, G. Vörös, Mater. Sci. Eng. A325 (2002) 255–260.
[8] M. Abbadi, P. Hähner, A. Zeghloul, Mater. Sci. Eng. A337 (2002) 194–201.

[9] Gy. Bérces, N.Q. Chinh, A. Juhász, J. Lendvai, J. Mater. Res. 13 (1998) 1411–1413.
[10] Gy. Bérces, N.Q. Chinh, A. Juhász, J. Lendvai, Acta Metall. 46 (1998) 2029–2037.
[11] N.Q. Chinh, F. Csikor, Zs. Kovács, J. Lendvai, J. Mater. Res. 15 (2000) 1037–1040.
[12] N.Q. Chinh, Gy. Horváth, Zs. Kovács, J. Lendvai, Mater. Sci. Eng. A324 (2002) 219–224.
[13] N.Q. Chinh, J. Gubicza, Zs. Kovács, J. Lendvai, J. Mater. Res. 19 (2004) 31–45.
[14] Gy. Horváth, N.Q. Chinh, J. Lendvai, J. Mater. Res. 20 (2005) 331–337.
[15] N.Q. Chinh, Gy. Horváth, Zs. Kovács, A. Juhász, Gy. Bérces, J. Lendvai, Mater. Sci. Eng. A409 (2005) 100–107.
[16] L.P. Kubin, Y. Estrin, Acta Metall. Mater. 38 (1990) 697–708.
[17] A. van den Beukel, U.F. Kocks, Acta Metall. Mater. 30 (1982) 1027–1034.
[18] F. Springer, Ch. Schwink, Scripta Metall. Mater. 32 (1995) 1771–1776.
[19] C.P. Ling, P.G. McCormick, Acta Metall. Mater. 38 (1990) 2631–2635.
[20] J. Balík, Mater. Sci. Eng. A316 (2001) 102–108.
[21] F. Springer, Ch. Schwink, Scripta Metall. Mater. 25 (1991) 2739–2744.
[22] C.P. Ling, P.G. McCormick, Acta Metall. Mater. 41 (1993) 3127–3131.
[23] M. Fellner, M. Hamerský, E. Pink, Mater. Sci. Eng. A 137 (1991) 157–161.
[24] K. Chihab, H. Ait-Amokhtar, K. Bouabdellah, Ann. Chim. Sci. Mater. 27 (2002) 69–75.
[25] P. Lukáč, J. Balík, F. Chmelík, Mater. Sci. Eng. A234–A236 (1997) 45–51.
[26] J.M. Reed, M.E. Walter, Mater. Sci. Eng. A359 (2003) 1–10.
[27] S. Kumar, H. Weinhandl, E. Pink, Mater. Sci. Eng. A212 (1996) 213–221.
[28] F. Springer, A. Nortmann, Ch. Schwink, Phys. Stat. Sol. (a) 170 (1998) 63–81.
[29] F. Chmelík, A. Ziegenbein, H. Neuhäuser, P. Lukáč, Mater. Sci. Eng. A324 (2002) 200–207.
[30] J. Gubicza, N.Q. Chinh, Z. Horita, T.G. Langdon, Mater. Sci. Eng. A387–A389 (2004) 55–59.
[31] U.F. Kocks, J. Eng. Mater. Technol. 98 (1976) 76–85.
[32] Y. Estrin, H. Mecking, Acta Metall. Mater. 32 (1984) 57–70.
[33] G.A. Malygin, Phys. Stat. Sol. (a) 119 (1990) 423–436.
[34] N.Q. Chinh, G. Horváth, Z. Horita, T.G. Langdon, Acta Mater. 52 (2004) 3555–3563.
[35] S.S. Woo, Y.R. Kim, D.H. Shin, W.J. Kim, Scripta Mater. 37 (1997) 1351–1358.
[36] D.A. Hughes, Acta Metall. Mater. 41 (1993) 1421–1430.
[37] M. Verdier, M. Janecek, Y. Brechet, P. Guyot, Mater. Sci. Eng. A248 (1998) 187–197.